UNIVERSITAT DE BARCELONA

Departament d'Astronomia i Meteorologia


# Astrophysical Studies on Open Clusters:

## NGC 1807, NGC 1817, NGC 2548 and NGC 2682

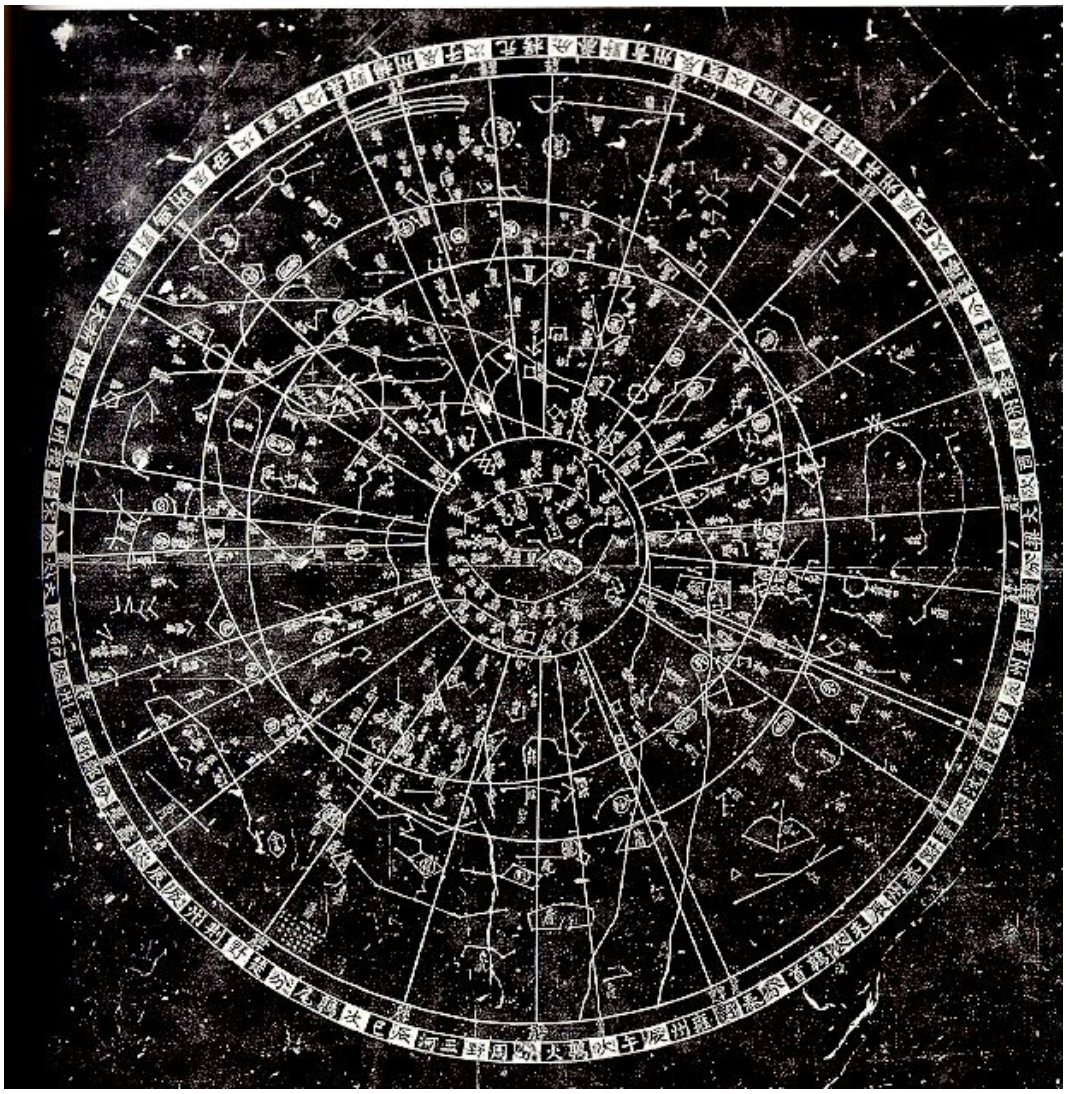

Memoria presentada por

**María de los Dolores Balaguer Núñez**

para optar al grado de

Doctora en Física

Barcelona, 31 de octubre de 2005

## 月夜

更深月色半人家，
北斗闌干南斗斜。
今夜偏知春氣暖，
蟲聲新透綠窗沙。

劉方平 (742)

### Moonlit Night

In the deep of the night, the moon lights up half the room,
Northern dipper and southern stars are beginning to descend.
This night I feel the coming of spring from the warm breeze,
Insects are newly calling throogh the window's drapes.

Liu Fangping (fl. 742)

# 3 NGC 1817 and NGC 1807: $uvby - H_\beta$ CCD Photometry and membership segregation

The study of the astrometry of the NGC 1817/NGC 1807 area in Section 2.3, gave as a result an unusually large size of the open cluster NGC 1817 and a very poor NGC 1807. As explained in Section 2.4, we decided to undertake a wide-field photometric study of the whole area, enhancing that way the astrometric-only membership analysis, and to derive the physical properties of the existing clusters.

Cuffey (1938) obtained extensive photographic photometry of stars in the NGC 1817 area in the blue and red bands down to a limiting magnitude of $R = 14$. Then Purgathofer (1961, 1964) performed a photometric study of the region, reaching $V = 14$. Harris & Harris (1977) obtained $UBV$ photographic photometry of 265 stars in the central area of this cluster down to a limit $V = 16.7$. Grocholski & Sarajedini (2002) used the $K$-band from 2MASS photometry as a distance indicator and unpublished $BVIK$ to compare different theoretical isochrones (Grocholski & Sarajedini 2003).

Mermilliod et al. (2003) showed photometry and radial velocity results for 88 red giant stars in the area, finding 39 members of NGC 1817 out to a distance of $27'$ from the cluster centre. A radius of at least twice as large as previously tabulated is then expected for NGC 1817.

In this Chapter[1] we discuss the results of the $uvby - H_\beta$ CCD photometric study of the area of NGC 1817 and NGC 1807, covering $65' \times 40'$ down to $V \sim 22$.

[1]This Chapter is based on: Balaguer-Núñez L., Jordi C., Galadí-Enríquez D., & Masana E., 2004a, A&A 426, 827

## 3.1 The Data

### 3.1.1 Observations

The photometric data were obtained in several observational runs at Calar Alto Observatory (Almería, Spain) and at Observatorio del Roque de los Muchachos (ORM, La Palma, Canary Islands, Spain).

Deep Strömgren CCD photometry of the area was performed at Calar Alto in January 1999 and January 2000 using the 1.23 m telescope of Centro Astronómico Hispano-Alemán (CAHA) and in February 1999 and January 2000 using the 1.52 m telescope of Observatorio Astronómico Nacional (OAN). Further data were obtained at ORM in February 2000 using the 2.5 m Isaac Newton Telescope (INT) of ING (equipped with the Wide-Field Camera, WFC), and in December 1998 and February 2000 using the 1 m Jakobus Kapteyn Telescope (JKT) of ING, with the $H_\beta$ filter.

The poor quality of the images obtained on the 1998/99 runs and in the OAN 2000 observations, due to adverse meteorological conditions, prevented us from making use of the data collected during those nights. A log of the observations, the total number of frames, exposure times, seeing conditions and chip specifications, is given in Tables 3.1 and 3.2. The frames form a mosaic that covers the area shown in the finding chart of the cluster (Figure 3.1).

We obtained photometry for a total of 7842 stars in an area of $65' \times 40'$ around NGC 1817 and NGC 1807, down to a limiting magnitude $V = 22$. Due to the lack of $H_\beta$ filter at the WFC-INT, it was only possible to measure it at the JKT and CAHA telescopes, thus limiting the spatial coverage of the mosaic with this filter.

Beside long, deep exposures, additional shorter exposures were obtained in order to avoid saturation of the brightest stars.

Table 3.1: Log of the observations

| Telescope | Date | Seeing($''$) | n. of frames | Exp. Times (s) | | | | |
|---|---|---|---|---|---|---|---|---|
| | | | | $u$ | $v$ | $b$ | $y$ | $H_\beta$ |
| 1.23 m CAHA | 1999/01/12-15 | (1) | 19 | 1900 | 800 | 400 | 400 | 2000 |
| 1.23 m CAHA | 2000/01/05-10 | 1.0-1.3 | 54 | 2200 | 1400 | 900 | 800 | 1400 |
| 1.52 m OAN | 1999/01/13-16 | (1) | 36 | 1900 | 800 | 400 | 400 | 2000 |
| 1.52 m OAN | 2000/02/07-14 | (1) | 23 | – | – | 900 | 800 | 1400 |
| 1 m JKT | 1998/12/11-14 | (1) | 81 | 2000 | 1200 | 800 | 700 | 1200 |
| 1 m JKT | 2000/02/02-06 | 0.9-1.3 | 37 | – | – | – | – | 2000 |
| 2.5 m WFC-INT | 2000/02/02-03 | 1.3 | 23 | 2000 | 2000 | 1200 | 500 | – |

(1) Poor weather conditions. Images not used in the final data.

Table 3.2: Chip specifications

| | 1.23 m CAHA | 1.52 m OAN | 2.5 m WFC-INT | 1 m JKT |
|---|---|---|---|---|
| Type: | SiTe2b | TK1024AB | 4× EEVi42-80 | SiTe2 |
| Dimensions: | 2048×2048 | 1024×1024 | 4× 2048×4100 | 2048×2048 |
| Pixel size: | $24\mu$=0.4$''$ | $24\mu$=0.4$''$ | $13.5\mu$=0.33$''$ | $24\mu$=0.33$''$ |
| Field of view: | $10' \times 10'$ | $6'.9 \times 6'.9$ | $34.2' \times 34.2'$ | $10' \times 10'$ |
| Gain: | 2.6e-/ADU | 6.55e-/ADU | 2.8 e-/ADU | 1.41e-/ADU |
| Read-out noise: | 6.0 e- | 6.4 e- | 7.7 e- | 7.5 e- |
| Dymamic range: | 65553 | 65536 | 65000 | 65000 |
| Typical bias level: | 154 | 470 | 1623 | 625 |
| Overscan region: | right | top | right-top-left | top-right |

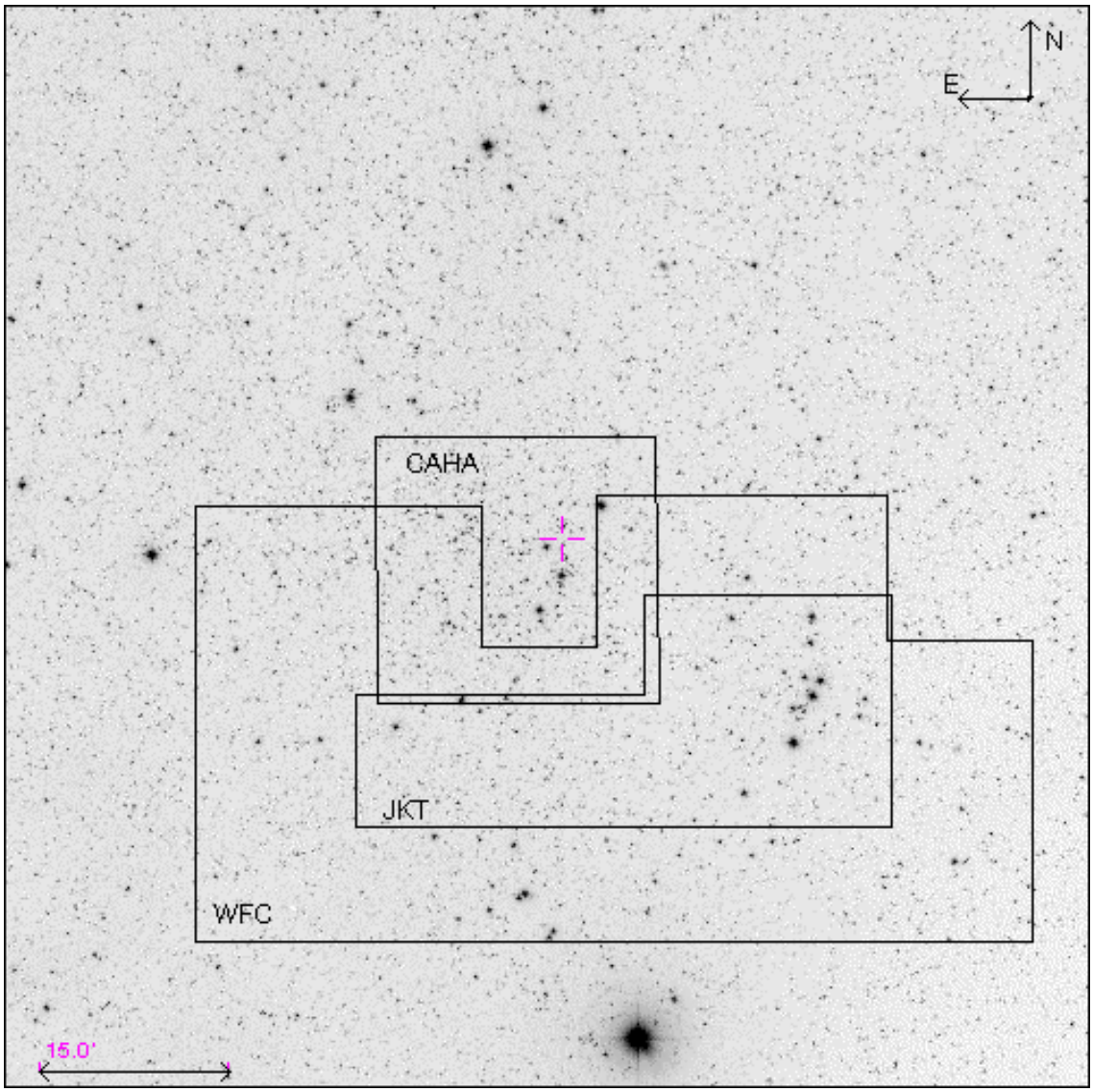


Figure 3.1: Finding chart of the area under study. The resulting area of the mosaic of images for each telescope is marked in black on an image of a plate (POSSI.E—optical R—.DSS1.417-LOW) plotted with Aladin (Bonnarel et al. 2000).

### 3.1.2 Reduction and transformation to standard system

#### 3.1.2.1 CAHA and JKT Data

Our general procedure has been to routinely obtain twilight sky flats for all the filters and a sizeable sample of bias frames (around 10) before and/or after every run. Flat fields are typically fewer in number, from five to ten per filter. Two or three dark frames of 2000 s were also taken. IRAF[2] routines were used for the reduction process as described below. Dome flats were taken to check shutter effects on the images of the OAN and CAHA telescopes where significant effects were previously noted (Galadí-Enríquez et al. 1994, Jordi et al. 1995). In the current configuration of all the telescopes used this effect is negligible.

The bias level was evaluated individually for each frame by averaging the counts of the most stable pixels in the overscan areas. The 2-D structure of the bias current was evaluated from the average of a number of dark frames with zero exposure time. Dark current was found to be negligible in all the cases. Flatfielding was performed using sigma clipped, median stacked, dithered twilight flats.

Our fields are not crowded. Thus, synthetic aperture techniques provide the most efficient measurements of relative fluxes within the frames and from frame to frame. We use the appropiate IRAF packages, and DAOPHOT and DAOGROW algorithms (Stetson 1987, 1990). We analysed the magnitude growth curves and determined the aperture correction with the IRAF routine MKAPFILE.

From a large number of frames with different FWHM, we applied an iterative procedure to obtain the instrumental magnitudes. In the first step, a preliminary value of the FWHM was used to detect the stars recorded in each frame. DAOPHOT and MKAPFILE were then used to obtain the instrumental photometry and the individual FWHM of each frame. In the second step, the detection of the stars was improved by using the individual FWHM given by DAOGROW. Again, DAOPHOT and MKAPFILE were used to obtain more accurate instrumental photometry and new individual FWHM. The iteration finishes when no new stars are detected and when the individual FWHM are the same as in the previous step. Two iterations

[2]IRAF is distributed by the National Optical Astronomy Observatories, which are operated by the Association of Universities for Research in Astronomy, Inc., under cooperative agreement with the National Science Foundation.

were enough in our case.

The same field was measured with both long and short exposure. Cross identification of stars among different frames was performed using the DAOMATCH and DAOMASTER programs (Stetson 1993). We retained only those stars detected in at least three filters, to enable the computation of two independent colours.

Equatorial coordinates were computed using the USNO-2 Catalogue (Monet et al. 1998) as reference stars. The region under study contains 2877 stars from this catalogue. Following Galadí-Enríquez et al. (1998c) the best fitting of these reference stars was a second order pair of equations.

#### 3.1.2.2 WFC-INT Data

After processing the WFC-INT frames as above, we found problems in the determination of the photometric zero point calibration for the 4 chips of the mosaic, basically due to gain differences between the A2D converters of the 4 CCDs. We decided to employ the pipeline specifically developed by the Cambridge Astronomical Survey Unit for WFC images from the INT, where the four chips are normalised to a common system in their level counts. The pipeline linearises, bias subtracts, gain corrects and flatfields the images. Catalogues are generated using algorithms described in Irwin (1985). The pipeline gives accurate positions in right ascension and declination linked to the USNO-2 Catalogue (Monet et al. 1998), and instrumental magnitudes with their corresponding errors. A complete description can be found in Irwin & Lewis (2001) and in `http://www.ast.cam.ac.uk/~wfcsur/index.php`.

#### 3.1.2.3 Transformation to standard system

Once the instrumental magnitudes and their errors were obtained, the next step was their transformation into the standard system.

The coefficients of the transformation equations were computed by a least squares method using the instrumental magnitudes of the standard stars and the standards magnitudes and colours in the $uvby - H_\beta$ system. Up to 68 standard stars from the cluster NGC 2682 (M 67; Nissen et al. 1987) were observed depending on the size of the field. Four to six short exposures in every filter were taken every night with a

magnitude limit of $V = 18$. Those standard stars with residuals greater than $2\sigma$ were rejected. Typically that involves a 10-15% of the standard stars, mainly variables from the M 67 field. Following Jordi et al. (1995), the reduction was performed for each night independently and in two steps.

The first step is to determine the extinction coefficients for each passband from the standard stars. To calculate these coefficients we make use of all the stars ($\approx$300) in the field of M 67, increasing the accuracy of our fit. The extinction coefficients for each night and filter are then calculated as the difference between the measurements as a function of the difference in airmasses. For instance, we have:

$$u_i - u_j = k_u(\chi_i - \chi_j) \tag{3.1}$$

where $u_i$,$u_j$ are the different measurements of the same star at different airmasses $\chi_i$,$\chi_j$. Analogous equations were used for the other passbands. Typical residuals are $\sigma = 0.008$ for the CAHA and JKT and $\sigma = 0.001$ for the WFC.

Because of the long exposure times, the suitable airmass value for each frame was obtained by integrating the instantaneous airmass throughout the exposure. Following Jordi et al. (1995) we approximated the integral by Simpson's rule with three points.

With the extinction coefficients fixed, the transformation to the standard system was completed in the next step, in which we used only the stars with known standard photometric values present in the field. The equations were as follows:

$$y' - V = a_1 + a_2(b - y) \tag{3.2}$$

$$(b - y)' = a_3 + a_4(b - y) \tag{3.3}$$

$$c_1' = a_5 + a_6(b - y) + a_7 c_1 \tag{3.4}$$

$$m_1' = a_8 + a_9(b - y) + a_{10} m_1 \tag{3.5}$$

$$H_\beta' = a_{11} + a_{12} H_\beta \tag{3.6}$$

were $a_i$ are the transformation coefficients and the $'$ indicates instrumental values.

In the CAHA images we decided to treat all the nights together —after correcting for atmospheric extinction— to fit those coefficients, and then to determine the zero point deviations from that fit for every night. For coherence, we refer those zero points to the precise results obtained with the WFC-INT, thanks to the generous overlap between the CAHA observations and the WFC-INT field.

Table 3.3: Number of stars observed ($N$) and mean internal errors ($\sigma$) as a function of apparent visual magnitude.

| $Vrange$ | $V$ | | $(b-y)$ | | $m_1$ | | $c_1$ | | $H_\beta$ | |
|---|---|---|---|---|---|---|---|---|---|---|
| | $N$ | $\sigma$ | $N$ | $\sigma$ | $N$ | $\sigma$ | $N$ | $\sigma$ | $N$ | $\sigma$ |
| 8- 9 | 3 | 0.011 | 3 | 0.068 | 3 | 0.012 | 3 | 0.042 | 2 | 0.007 |
| 9-10 | 8 | 0.010 | 8 | 0.030 | 8 | 0.041 | 8 | 0.043 | 4 | 0.014 |
| 10-11 | 18 | 0.008 | 18 | 0.007 | 16 | 0.014 | 14 | 0.014 | 8 | 0.039 |
| 11-12 | 36 | 0.010 | 36 | 0.013 | 33 | 0.016 | 32 | 0.022 | 19 | 0.026 |
| 12-13 | 102 | 0.011 | 102 | 0.014 | 100 | 0.025 | 95 | 0.026 | 65 | 0.018 |
| 13-14 | 167 | 0.009 | 167 | 0.011 | 165 | 0.023 | 158 | 0.025 | 86 | 0.018 |
| 14-15 | 300 | 0.009 | 299 | 0.014 | 297 | 0.019 | 292 | 0.022 | 151 | 0.028 |
| 15-16 | 471 | 0.009 | 471 | 0.016 | 467 | 0.024 | 458 | 0.031 | 216 | 0.024 |
| 16-17 | 833 | 0.014 | 833 | 0.026 | 799 | 0.038 | 761 | 0.047 | 355 | 0.027 |
| 17-18 | 1110 | 0.021 | 1110 | 0.036 | 945 | 0.050 | 843 | 0.058 | 317 | 0.037 |
| 18-19 | 1140 | 0.019 | 1139 | 0.038 | 882 | 0.045 | 734 | 0.055 | 36 | 0.036 |
| 19-20 | 1204 | 0.012 | 1204 | 0.029 | 991 | 0.036 | 565 | 0.056 | | |
| 20-21 | 1119 | 0.017 | 1119 | 0.037 | 867 | 0.055 | 143 | 0.072 | | |
| 21-22 | 1007 | 0.045 | 1007 | 0.064 | 387 | 0.090 | 5 | 0.092 | | |
| 22-23 | 252 | 0.090 | 252 | 0.121 | 32 | 0.139 | | | | |
| Total | 7770 | | 7768 | | 5992 | | 4111 | | 1259 | |

The internal errors of the individual measurements were computed as described by Jordi et al. (1995), taking into account the errors in the instrumental magnitudes on the one hand, and the errors in the transformation equations on the other hand. Final magnitudes, colours and errors were obtained by averaging the individual measurements of each star using the internal error for weighting (Galadí-Enríquez et al. 1998c, Rosselló et al. 1985). The final errors as a function of apparent visual magnitude are given in Table 3.3 and plotted in Figure 3.2. The structure in the magnitude dependence is owed to the mosaic of images from different nights and different telescopes having different limiting magnitude.

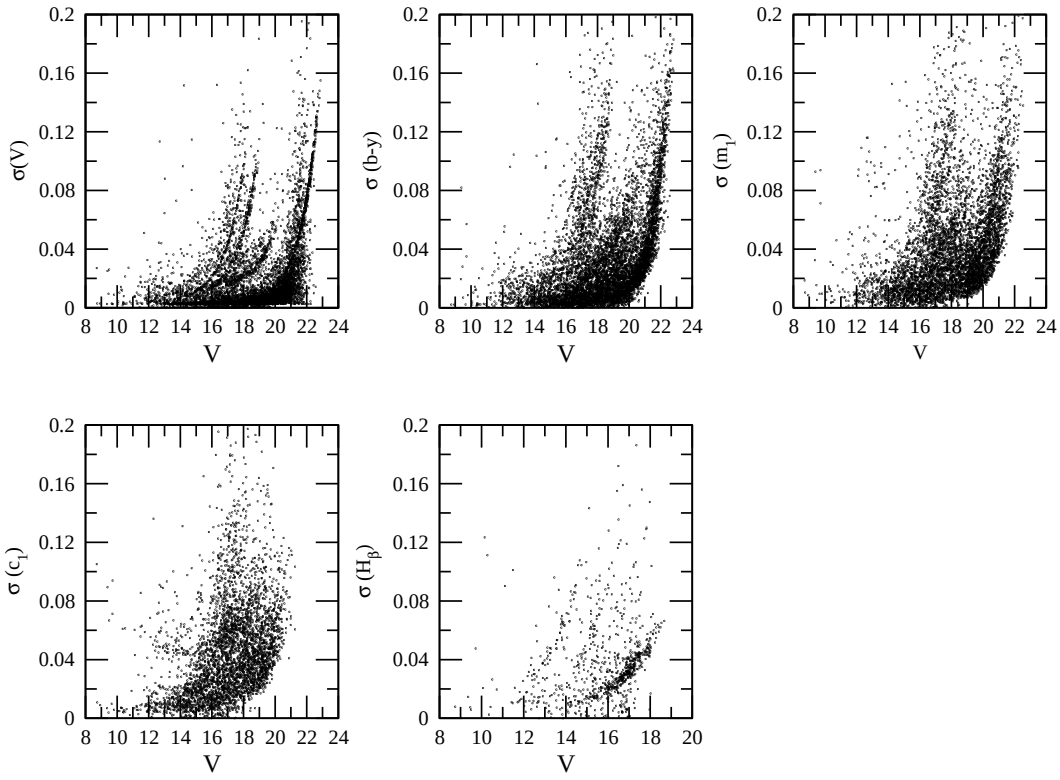


Figure 3.2: Mean internal errors of magnitude and colours as a function of the apparent visual magnitude, $V$, for all observed stars in NGC 1817 region. The structure in the magnitude dependence is owed to the mosaic of images from different nights and different telescopes having different limiting magnitude.

Table 3.4[3] lists the $u, v, b, y, H_\beta$ data for all 7842 stars in a region of $65' \times 40'$ around the open cluster NGC 1817 (Figure 3.1). Star centres are given as frame $(x, y)$ and equatorial ($\alpha_{\rm J2000}$,$\delta_{\rm J2000}$) coordinates. Given the large area coverage and depth of our photometry, a new numbering system for stars in this field is introduced. An identification number was assigned to each star following the order of increasing right ascension. Column 1 is the ordinal star number; columns 2 and 3 are $\alpha_{\rm J2000}$ and $\delta_{\rm J2000}$; columns 4 and 5 are the respective $x$, $y$ coordinates in arcmin; columns 6 and 7 are the $(b-y)$ and its error, 8 and 9 the $V$ magnitude and its error, 10 and 11 the $m_1$ and its error, 12 and 13 the $c_1$ and its error, and 14 and 15 the $H_\beta$ and its error. In column 16, stars considered candidate members (Section 3.2.2.) are labelled 'M', while those classified as non-members show the label 'NM'.

The cross-identification of stars in common with the astrometry (Chapter 2), BDA (`http://obswww.unige.ch/WEBDA`), Hipparcos (ESA, 1997), Tycho-2 (Høg et al. 2000) and USNO-2 (Monet et al. 1998) catalogues is provided in Table 3.5[4].

### 3.1.3 Comparison with previous photometry

Only four stars in the field of NGC 1817 have been previously studied using Strömgren photometry, in the range of $V = 9.5$ to 12.9. Maitzen et al. (1981) performed a photometric search for Ap stars among Blue Stragglers in open clusters, with mean errors of less than 0.01. Mean differences in the sense ours minus others are: 0.03 ($\sigma = 0.04$) in $V$, 0.02 ($\sigma = 0.04$) in $b-y$, $-0.03$ ($\sigma = 0.07$) in $m_1$ and 0.00 ($\sigma = 0.03$) in $c_1$ for the 4 stars in common.

On the other hand, the $V$ magnitude derived from the $y$ filter can be compared with the published broadband data. The recent study of radial velocities of red giants in the area by Mermilliod et al. (2003) included photoelectric photometry of 25 stars. We have 22 common stars with the photoelectric photometry of Harris & Harris (1977) and 19 common stars with Purgathofer (1964), up to $V = 16$. The corresponding mean differences in $V$, in the sense ours minus others are: $-0.01$ ($\sigma = 0.03$), $-0.01$ ($\sigma = 0.04$) and $-0.01$ ($\sigma = 0.05$), respectively. Transformation between $B-V$ and $b-y$ from several authors (see Moro & Munari, 2000) fails to cover the

[3]Table 3.4 is available in electronic form from CDS via anonymous ftp to cdsarc.u-strasbg.fr (130.79.128.5) or via `http://cdsweb.u-strasbg.fr/cgi-bin/qcat?J/A+A/426/827`

[4]Table 3.5 is available in electronic form from CDS via anonymous ftp to cdsarc.u-strasbg.fr (130.79.128.5) or via `http://cdsweb.u-strasbg.fr/cgi-bin/qcat?J/A+A/426/827`

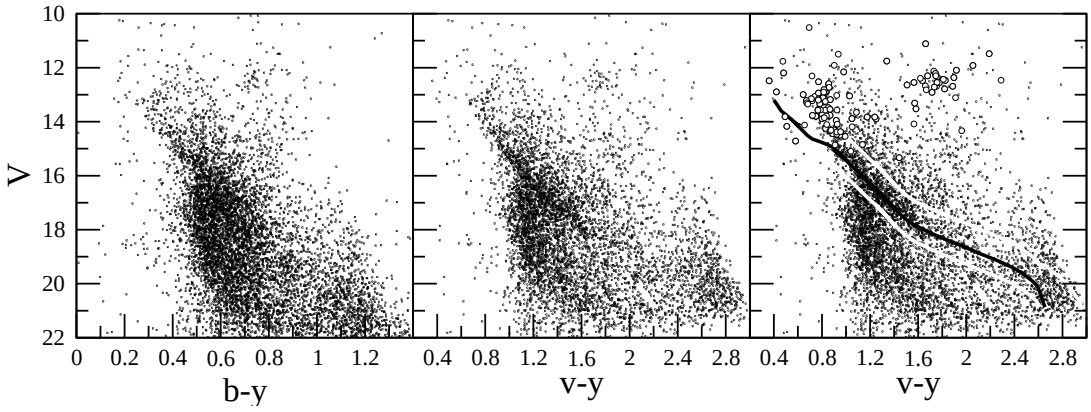


Figure 3.3: The colour-magnitude diagram of the NGC 1817 area. Empty circles in the right figure are the astrometric members from Chapter 2. Black line is a shifted ZAMS, with the chosen margin for candidate members ($V+0.5$,$V-1$) in white lines. See text for details.

whole range under study. Making use of merged broadband photometry, we can find a linear relation between the two indices: $B-V = (1.719\pm0.035)(b-y) - (0.170 \pm 0.024)$, $N = 62$. The standard deviation of the residuals about the mean relation is 0.055, where the typical uncertainty in $B-V$ is 0.02 and in $b-y$ is 0.014.

## 3.2 Colour-Magnitude diagrams

We use the $V$ vs $(v-y)$ colour-magnitude diagram for our study. As Meiborn (2000) stated, the colour-magnitude diagram based on this colour index defines the main-sequence of a cluster significantly better than the traditional $V$ vs $(b-y)$ diagram (Figure 3.3 left and centre). The fact that the reddening vector runs parallel to the cluster sequence in this diagram allows a much better separation of cluster and field stars.

The observational colour-magnitude diagram for all the stars in the studied area (Figure 3.3) displays a fairly well defined main sequence. Specially outstanding against the field background is the red giant clump and the main sequence between $0.8 < (v-y) < 1.8$.

### 3.2.1 Non-parametric member segregation in the photometric plane

The non-parametric method for member segregation applied to the proper motion plane in Section 2.6.2 can be generalised, in principle, to any observational space (see e.g. Section 2.6.3). Particularly, it can be applied to the photometric observational colour-magnitude diagram, as done by Galadí-Enríquez et al. (1998a).

The observational colour-magnitude diagram of the area under study shows an outstanding main sequence related to the cluster present in the zone. This photometric contrast can be used to assign photometric membership probabilities through the kernel estimator method. In the kinematic and spatial planes, both coordinates had the same physical meaning. But in the photometric plane, the different meaning of the variables (magnitude and colour) requires a normalisation of coordinates previous to the calculation of empirical frequency functions. This is the only difference in the treatment of the photometric plane with respect to the astrometric plane used in Chapter 2. The normalisation was done scaling the coordinate axis to get zero mean, and standard deviation equal to unity.

The cluster photometric empirical frequency function $\Psi_c^p$ (where "p" stands for "photometry") was computed from the mixed function, $\Psi_{c+f}^p$, subtracting from it the field contribution $\Psi_f^p$. The photometric frequency function of the selected field region, $\Psi_f^p$, can be assumed to represent the field contribution in the cluster region, affected only by a scale factor.

For a star placed at grid node $\{[V_i,(b-y)_j]; i,j = 1,...,N_c\}$, the photometric probability of it being a cluster star is:

$$P_c^p[V_i,(b-y)_j] = \frac{(\Psi_{c+f}^p[V_i,(b-y)_j] - \Psi_f^p[V_i,(b-y)_j])}{\Psi_{c+f}^p[V_i,(b-y)_j]} \tag{3.7}$$

We cannot define the same circle for the cluster and outside field used in the kinematic and spatial planes, since the area covered by the photometry is smaller ($65' \times 40'$) than the area covered by the astrometry of Chapter 2. Thus we have to find suitable areas for the mixed and the field functions. We tried different configurations of the PDF, $\psi_{c+f}^p$, using a central area of different sizes and for $\psi_f^p$ an area far from the centre and apparently clean enough of cluster members, but the results were not satisfactory and several drawbacks to the method appeared.

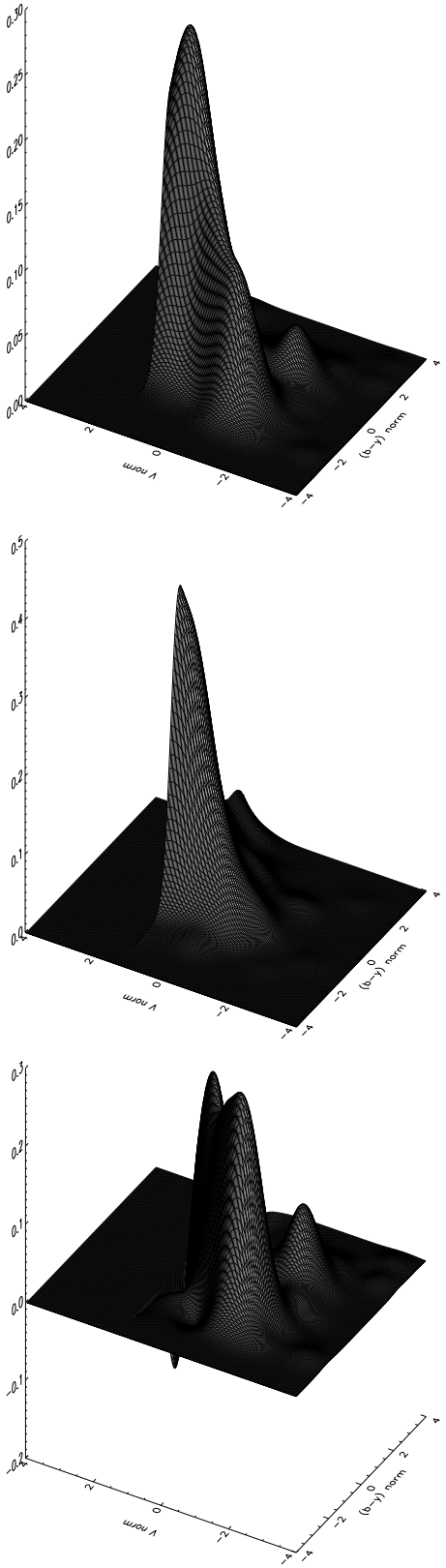


Figure 3.4: Photometric empirical PDF's. Top: $\psi^p_{c+f}$ (mixed sample) from a square of side 15′. Centre: $\psi^p_f$ (field population) from a field in a corner area of radius 10′. Bottom: $\psi^p_c$ (non-field, or cluster population). Axis are in normalised coordinates. Note that the magnitue axis is reversed respect to the usual orientation.

Figure 3.4 displays one of those tries with the empirical photometric PDF's: $\psi^p_{c+f}$ for the mixed sample in a square of side $15'$; $\psi^p_f$ for the field from a corner area with radius $10'$; and $\psi^p_c$ for the non-field or cluster population, all resulting after normalizing their respective frequency functions. The sample brightness cutoff at $V = 18$ corresponds to normalised magnitude $V_{norm} \sim 1$. The cluster main-sequence and red clump are well-defined and the behaviour of the faint end of the field PDF shows a clear tendency to exponential grow, as expected. But the non-field PDF shows obvious problems and drawbacks of the method when applied to our data:

- First, the ratio of cluster members (that will be extrapolated to all the area) strongly depends on the choice of a radius for the mixed distribution.
- Second, the overabundance of negative points (Figure 3.4, bottom) points towards possible problems with the limiting magnitude of the farthest area chosen as representative of the field with respect to the limiting magnitude of the central region. But even taking a brighter magnitude limit the situation does not improve much.
- Third and most important, the difference in the behaviour of the errors (its dispersion) and its structure (see Figure 3.2) due to different magnitude limits, on the two areas chosen induces irresoluble problems and non-physical results.

We have also tried different colour planes (i.e. $V$, $v - y$) with similar results. Other tries involving Galaxy models taken from Besançon (Robin et al. 2003) to represent the field are also unable to imitate the distribution of errors of our data. The shape of the modeled field changes greatly with the model of the errors.

To make use of the kernel estimator method a highly-uniform quality of data is necessary, plus an area free of cluster members. We are unable to get realistic photometric membership probabilities from this technique. Next Section will make use of the photometric information in a classical way.

### 3.2.2 Selection of candidate member stars

A selection of probable member stars up to the limiting magnitude of our sample can be obtained combining astrometric with photometric criteria. Unfortunately, proper

motions (Chapter 2) and radial velocities (Mermilliod et al. 2003) are only available for the brightest stars in the area. Photometric measurements help to reduce the possible field contamination in the proper motion membership —among bright stars—, as well as to enlarge the selection of members towards faint magnitudes.

Among those astrometric member stars, we find 13 stars that are not compatible with the sequence of the cluster outlined in the colour-magnitude diagram. Radial velocity information is also taken into account, to reject stars with radial velocities incompatible with membership and to include stars considered members by Mermilliod et al. (2003) and compatible with membership according to our photometric data. Our astrometric study —based on proper motions from plates—, and thus its segregation of member stars, has a limiting magnitude of $V = 14.5$. From this point down to $V = 21$ we construct a ridge line following a fitting of the observational ZAMS (Crawford 1975, 1978, 1979, Hilditch et al. 1983, Olsen 1984) in the $V - (v - y)$ diagram. A selection of stars based on the distance to this ridge line is then obtained. The chosen margin for candidates includes all the stars between $V + 0.5$ and $V - 1$ from the ridge line, as shown in the right panel of Figure 3.3. The margins were chosen to account for observational errors and the presence of multiple stars.

This preliminary photometric selection is refined in the colour-colour diagrams (Figure 3.5) with the help of the standard relations from the same authors. A final selection of 1592 stars in the area is plotted in Figure 3.5 as empty circles in the $[m_1] - [c_1]$, $m_1 - (b - y)$, $c_1 - (b - y)$ and $[c_1] - H_\beta$ diagrams.

## 3.3 Fundamental parameters of the cluster

As already discussed in Chapter 1, narrow and intermediate passband photometry constitutes a useful technique for classification of the stars (Strömgren 1966; Philip et al. 1976). The stars of the area selected as possible cluster members are classified into photometric regions and their physical parameters determined. The algorithm uses $uvby - H_\beta$ photometry and standard relations among colour indices for each of the photometric regions of the HR diagram. Masana (1994) provide improvements to the algorithm classification and parametrisation described in Jordi et al. (1997) and Figueras et al. (1991). Improvements concern the inclusion of a grid of temperatures and gravities dependent on metallicity, the determination of masses and radii as well

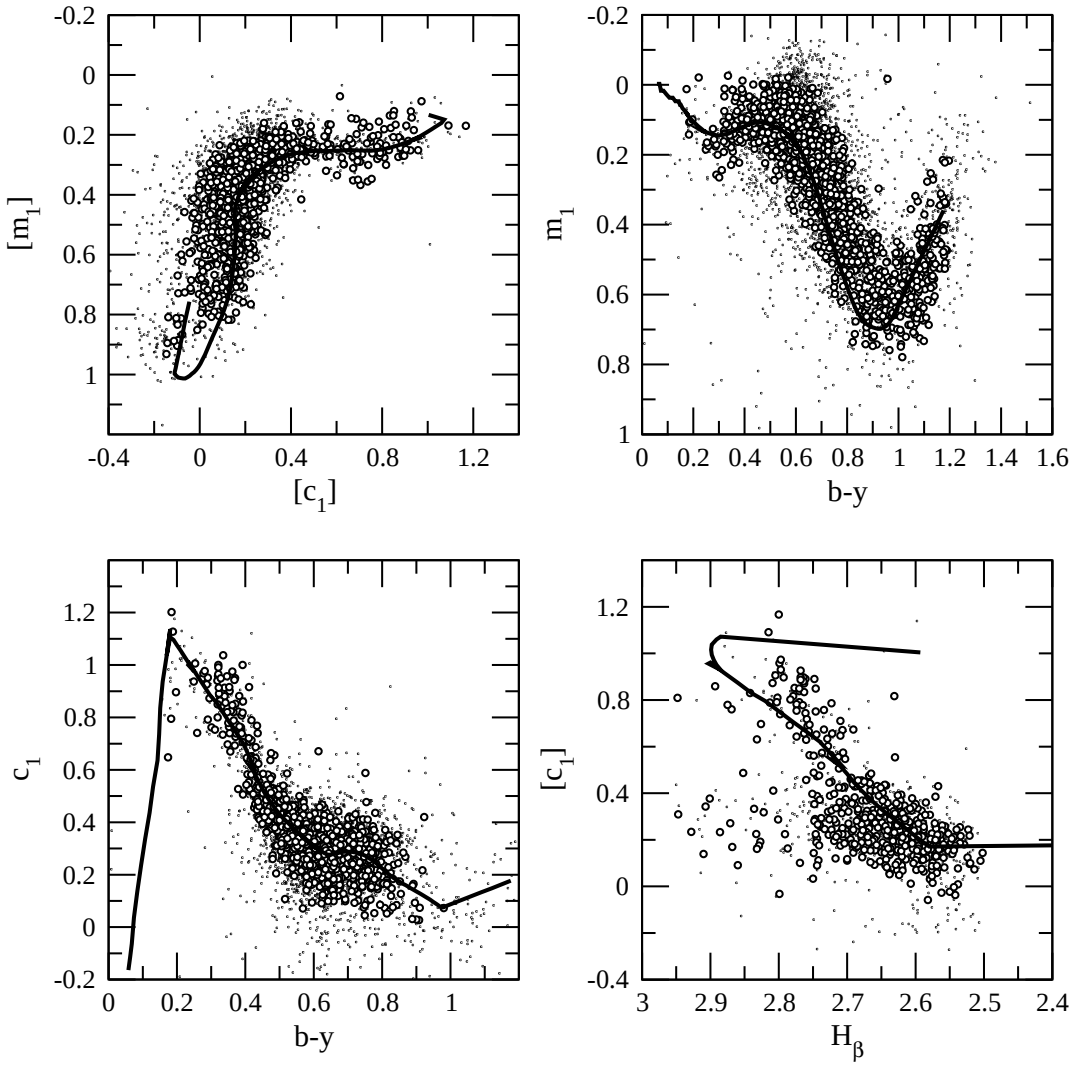


Figure 3.5: The colour-colour diagrams of NGC 1817. Empty circles denote candidate members of NGC 1817, chosen with astrometric and non-astrometric criteria as explained in Section 3.2.2. The thick line is the standard relation shifted $E(b-y) = 0.19$ when necessary.

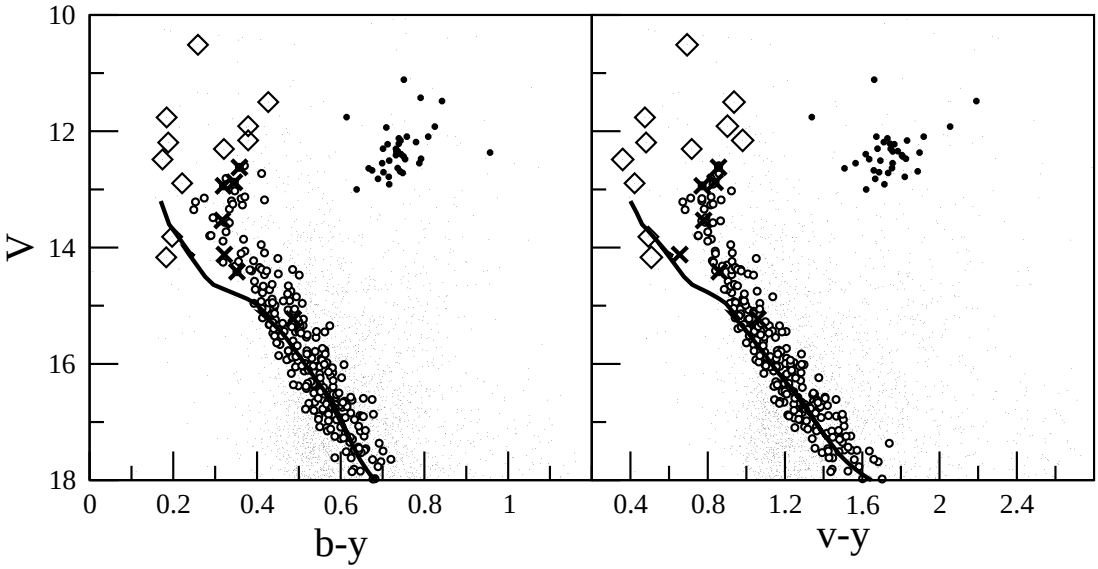


Figure 3.6: Colour-magnitude diagram with the subset of 264 stars used to derive the physical parameters in empty circles, the red giants in full circles, blue stragglers in diamonds and $\delta$ Scuti in crosses. Field stars are in dots. The thick line is the ZAMS, shifted in extinction and distance modulus.

as the detection of peculiar stars.

Absolute magnitude, effective temperature and gravity as well as the corresponding reddening, distance modulus, metallicity and a raw spectral type and luminosity class are calculated for each star. Typical errors are 0.25 mag in $M_V$, 0.15 dex in [Fe/H], 270 K in $T_{\rm eff}$, 0.18 dex in $\log g$ and 0.015 mag in $E(b-y)$. Even if the result for the physical parameters for a given star would be inaccurate —mainly due to peculiarity, emission lines or binary character—, the high proportion of "well-behaved" stars makes it possible to ascertain the physical parameters of the cluster.

The fundamental parameters of NGC 1817 from Chapters 2 and the present one, are resumed in Table 3.8.

### 3.3.1 Distance, reddening and metallicity

Only 525 stars among the 1592 candidate members have $H_\beta$ measurements. So the computation of physical parameters is only possible for that subset. Red giant stars are outside of the validity of the calibrations. Excluding peculiar stars and those

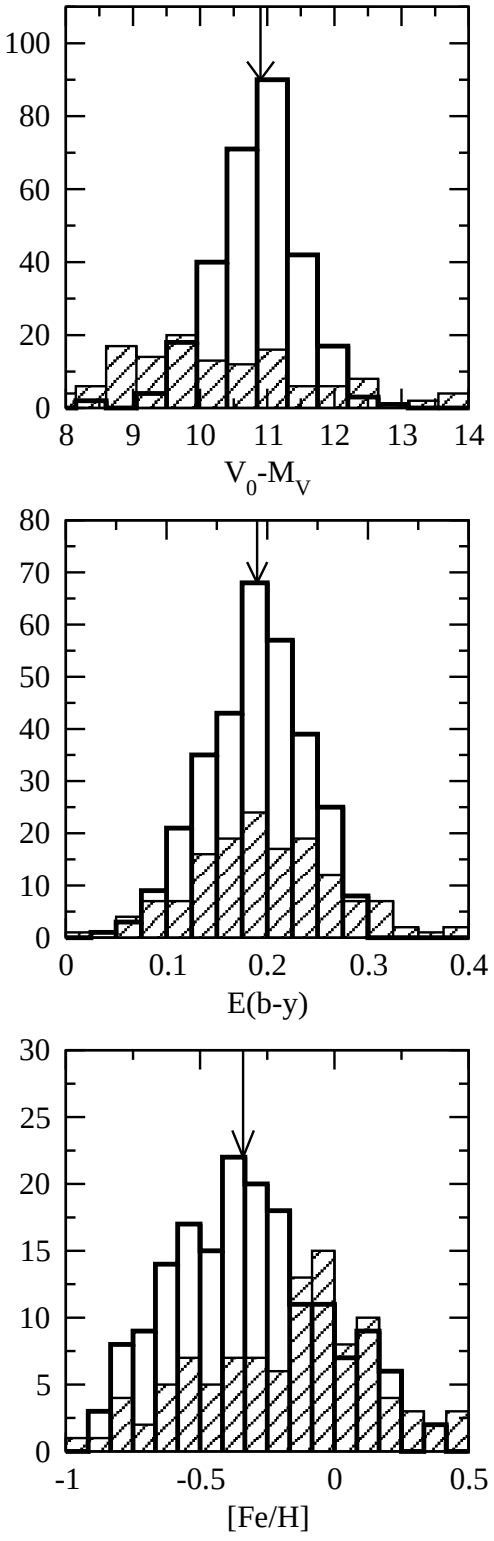


Figure 3.7: The histograms of the distance modulus, reddening and metallicity of the selected member stars of NGC 1817 (white), and the corresponding ones for the stars in the NGC 1807 area (dashed). The arrows indicate the mean values adopted for the cluster NGC 1817.

with inconsistence among their photometric indices, we compute an average with a $2\sigma$ clipping to that subset and only 264 stars remain (Figure 3.6). We found a reddening value of $E(b-y) = 0.19\pm0.05$ (corresponding to $E(B-V) = 0.27$) and a distance modulus of $V_0 - M_V = 10.9\pm0.6$. Metallicity is better calculated studying only the 196 F and G stars in our sample, inside the validity range of the calibrations of Schuster & Nissen (1989, see Masana et al. 1994 for more details). We found a value of [Fe/H] $= -0.34\pm0.26$. Figure 3.7 shows these results.

Our results are consistent with previous results. Harris & Harris (1977) give a reddening value of $E(B-V) = 0.28\pm0.03$ and a distance modulus of $11.3\pm0.3$. Friel & Janes (1993) give a value of [Fe/H] $= -0.39\pm0.04$ ($N = 4$) on the basis of moderate-resolution spectra, while Taylor (2001) reexamines the errors in these data and concludes a lower value of [Fe/H] $= -0.42\pm0.07$. Friel et al. (2002) give a recalibrated value of [Fe/H] $= -0.29\pm0.05$ based on 3 stars. Twarog et al. (1997) find an $E(B-V) = 0.26$, an [Fe/H] $= -0.27\pm0.02$ and $V_0 - M_V = 11.34$ based on main-sequence fitting. Dutra & Bica (2000) using DIRBE/IRAS 100 $\mu m$ dust emission integrated throughout the Galaxy derive a value of $E(B-V)_{FIR} = 0.33$.

### 3.3.2 Age

The recent publication by Clem et al. (2004) of empirically constrained colour-temperature relations in the Strömgren system allows the transformation of isochrones from the theoretical to the observational colour-magnitude diagram. Several sets of isochrones have been used to analyse our results. The best fitting is found for the Schaerer et al. (1993) isochrones. Figure 3.8 shows isochrones of $Z = 0.008$ shifted by a reddening of 0.19 and an apparent distance modulus of 11.6. We found a best estimation of the age of $\log t = 9.05\pm0.05$. Harris & Harris (1977) give a Hyades-age for this cluster: 0.8 Gyr ($\log t = 8.9$). But a recent determination of ages of old open clusters (Salaris et al. 2004) gives an age of $1.12\pm0.18$ Gyr based on the morphological age index provided by Janes & Phelps (1994) but on a new highly homogeneous and reliable calibration in terms of absolute ages. Our age determination, 1.1 Gyr, agrees very well.

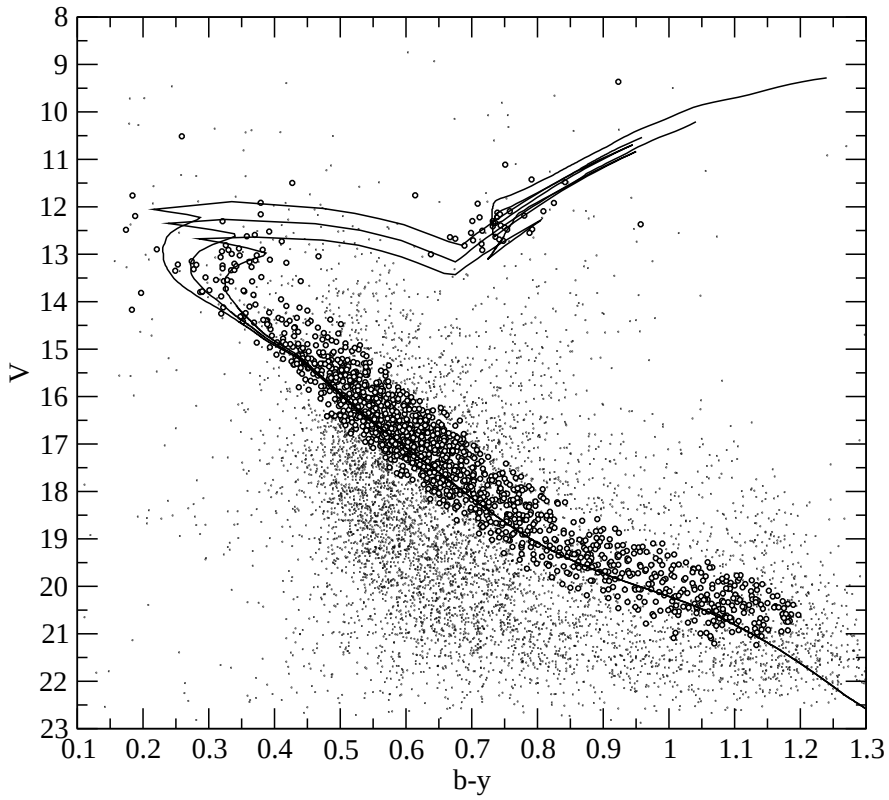


Figure 3.8: Geneva isochrones (Schaerer et al. 1993) of $\log t$ 8.9, 9.0 and 9.1 and $Z = 0.008$. The adopted reddening and apparent distance modulus are 0.19 and 11.6, respectively. Empty circles denote candidate members of NGC 1817.

Table 3.6: Blue Stragglers in NGC 1817, with their membership from Chapter 2. The first seven are from the catalogue of Ahumada & Lapasset (1995). The last six have been classified in this work.

| Id. | HH | $(b-y)$ | $V$ | $P$ |
|---|---|---|---|---|
| 7091 | 2045 | 0.321±0.0059 | 12.305±0.0176 | M |
| 157 | 2090 | 0.209±0.0097 | 13.112±0.0000 | NM |
| 389 | 2072 | 0.188±0.0011 | 12.195±0.0009 | M |
| 387 | 2110 | 0.184±0.0051 | 11.762±0.0056 | M |
| 7467 | 2020 | 0.221±0.0126 | 12.896±0.0074 | M |
| 7746 | 1073 | 0.421±0.0147 | 12.270±0.0123 | NM |
| 7310 | 3001 | 0.197±0.0210 | 13.816±0.0309 | M |
| 1126 | | 0.174±0.0027 | 12.486±0.0029 | M |
| 390 | | 0.379±0.0036 | 12.157±0.0048 | M |
| 388 | | 0.379±0.0101 | 11.914±0.0035 | M |
| 45 | | 0.427±0.0014 | 11.498±0.0172 | M |
| 6161 | | 0.259±0.0023 | 10.514±0.0027 | M |
| 7332 | | 0.183±0.1662 | 14.169±0.0965 | M |

### 3.3.3 Blue stragglers and pulsating stars

There are seven known blue stragglers in our photometry from the catalogue of blue stragglers in open clusters (Ahumada & Lapasset 1995). But two of them (HH2090, HH1073) are not proper motion members. From a sample of 18 clusters, Wheeler (1979) found a ratio of the number of stragglers to giants of from 1/3 to 1/4. Having 39 confirmed red giants in the cluster (Mermilliod et al. 2003) we should expect between 10 and 13 blue stragglers. The location in our colour-magnitude diagram of six blue stars that are astrometric members according to Chapter 2 lead us to classify them also as blue stragglers. Their photometry and astrometric segregation from Chapter 2 are listed in Table 3.6.

Open clusters with an age around 1 Gyr, with the turn off on the instability strip, seem to have the largest number of pulsators. There are seven known $\delta$ Scuti stars in the area (Frandsen & Arentoft 1998). Five of them have absolute proper

Table 3.7: Physical parameters of the known $\delta$ Scuti stars in the NGC 1817 area, with the membership segregation from Chapter 2.

| Id. | $E(b-y)$ | $(b-y)_0$ | $V_0$ | $M_V$ | $V_0 - M_V$ | $T_{eff}$ | $\log g$ | $M/\mathrm{M}_\odot$ | $R/\mathrm{R}_\odot$ | $P$ |
|---|---|---|---|---|---|---|---|---|---|---|
| 154 | 0.179 | 0.167 | 12.116 | 0.57 | 11.55 | 7105 | 3.22 | 2.328 | 4.613 | M |
| 155 | 0.160 | 0.160 | 12.257 | 3.95 | 11.44 | 7199 | 3.35 | 2.200 | 3.858 | M |
| 167 | 0.211 | 0.106 | 12.631 | 1.77 | 10.86 | 7794 | 3.92 | 2.035 | 2.545 | NM |
| 184 | 0.216 | 0.136 | 13.494 | 3.30 | 10.20 | 7731 | 4.44 | 1.588 | 1.369 | – |
| 211 | 0.227 | 0.260 | 14.256 | 3.95 | 10.31 | 6780 | 4.72 | 1.246 | 0.972 | – |
| 7298 | 0.168 | 0.154 | 13.405 | 2.77 | 10.63 | 7502 | 3.79 | 1.461 | 1.121 | M |
| 7615 | 0.158 | 0.200 | 11.946 | 1.37 | 10.58 | 6917 | 3.44 | 2.007 | 3.376 | M |

motions and membership probabilities from Chapter 2. We have calculated the physical parameters for these stars and we are able to confirm the membership of four of them (Table 3.7).

### 3.3.4 Dimension and mass

We have found 169 members out of a sample of 722 stars (23%) in an area of $1\overset{\circ}{.}5 \times 1\overset{\circ}{.}5$ covered by our astrometry study with magnitude limit of $V_{\mathrm{lim}} = 14.5$. Following Galadí-Enríquez et al. (1998a), a good way of estimating cluster sizes is to determine the radius of the circle that contains half the total number of cluster members. This half-sample radius would be an underestimation of the true half-sample radius, if mass segregation is present in the cluster. We calculate this half-sample radius from the astrometric selection that covers a more complete area of the cluster than the photometric study. The first step is to calculate the real centre of the cluster from the list of members. Then we measure the radius that contains half the members, what gives a radius of $r_{\mathrm{h}} = 11.75'$. Taking the calculated distance of 1800 pc, it means a half-sample radius of 6.0 pc. From the photometry study we cover a smaller area ($65' \times 40'$) but to a much deeper magnitude ($V = 21$), and found 1592 members out of 6512 (24%).

The stellar density was taken from the central density of the cluster given by the

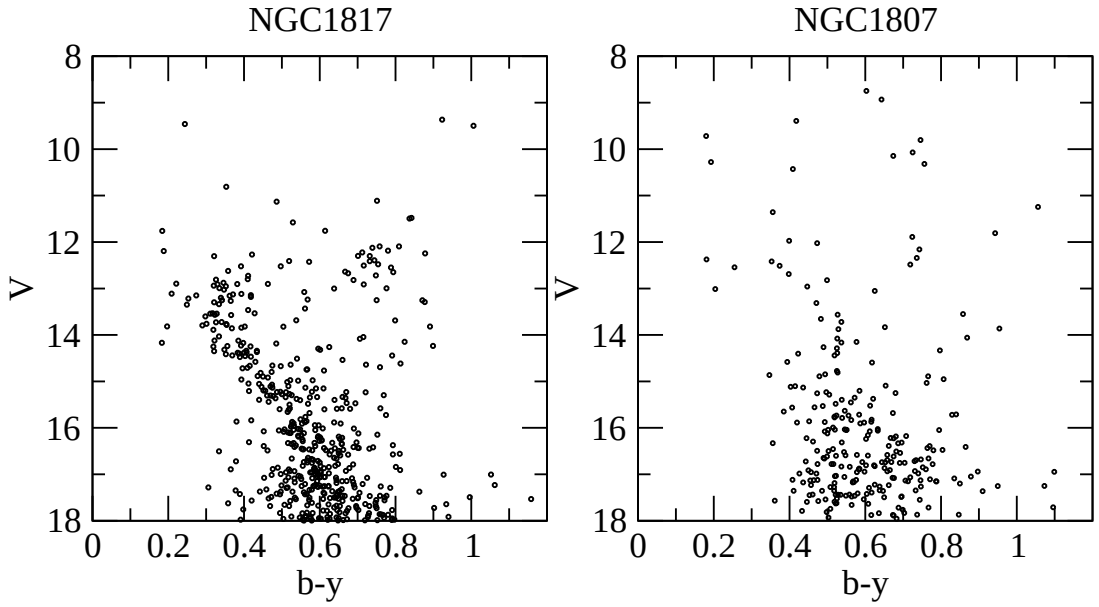


Figure 3.9: The colour-magnitude diagram of stars in an area of 15′ around the nominal centres of NGC 1817 and NGC 1807.

photometry in a radius of 9′ (chosen to ensure the given limiting magnitude): $\sigma = 0.72$ stars pc$^{-3}$ which corresponds to a mean space density $\rho = 0.83$ M$_\odot$ pc$^{-3}$.

We can calculate the total mass of the cluster only as a lower limit, restricted by our magnitude completeness and spatial coverage. The most recent isochrones computed by Pietrinferni et al. (2004) have been used to derived individual masses of the cluster members, relating each star with its closest point in the isochrone. This way we have not taken into account the binary contribution supposing only single stars. The minimum total mass is thus 1400 M$_\odot$. There are no previous mass estimations for this cluster.

## 3.4 NGC 1807: not a real physical open cluster

Comparison of the colour-magnitude diagram of the area around NGC 1807 and the centre of the open cluster NGC 1817, Figure 3.9, already shows a lack of a reliable main sequence for NGC 1807.

The star HD 33428, one of the brightest stars in the area of NGC 1807 ($V =$

8.5), has DDO observations (Yoss et al. 1981, Piatti et al. 1995), but proper motion studies (Chapter 2 and Hipparcos Catalogue, ESA 1997) show that it cannot belong to NGC 1807. Even in the case of NGC 1807 being a real cluster, this star is a high proper motion star.

The comparison of the result of our study of the physical parameters of NGC 1817 with a study of a sample of 200 stars in the area of NGC 1807 (Figure 3.7, shaded histogram), shows that the lack of a clear trend is unambiguous.

Chapter 2 also supports the idea of a unique and very extended cluster in the area, showing no hint of two kinematically distinct clusters in the area.

The results from Mermilliod et al. (2003) of radial velocities of red giants in the area also agree with there being only one and very extended cluster. There are six stars from Mermilliod et al. (2003) list in the NGC 1807 area. Two of them (M1152, M1208) are members of NGC 1817 and the other four (M598, M682, M1153, M1161) have discordant radial velocities (+74.51, +111.53, +28.49, +11.71 km $s^{-1}$).

We can conclude that there is no photometric nor astrometric evidence supporting the existence of a real cluster NGC 1807.

Table 3.8: Fundamental parameters of NGC 1817

| | |
|---|---|
| Identifiers | NGC 1817, C 0509+166, Collinder 60 |
| | NGC 1807 (being part of) |
| Position (J2000.0) | $\alpha = 5^{\rm h}12^{\rm m}.1$, $\delta = +16°42'$ |
| | $l = 186°.13$, $b = -13°.12$ |
| | in Taurus |
| Distance | $V_0 - M_V = 10.9 \pm 0.6$ |
| | $d = 1800$ pc |
| | $z = -405$ pc |
| Half-sample radius | $r_{\rm h} = 11.75'$ (6 pc) |
| Proper motion | $\mu_\alpha \cos\delta = 0.29 \pm 0.10$ mas yr$^{-1}$ |
| | $\mu_\delta = -0.96 \pm 0.07$ mas yr$^{-1}$ |
| Reddening | $E(b-y) = 0.19 \pm 0.05$ |
| | $E(B-V) = 0.27 \pm 0.07$ |
| Age | $\log t = 9.05 \pm 0.05$ |
| | $t = 1.1 \pm 0.1$ Gyr |
| Metallicity | [Fe/H] $= -0.34 \pm 0.26$ |
| Membership | $N$(M) = 169 ($V_{\rm lim} \sim 14.5$) in an area of $1°.5 \times 1°.5$ |
| | $N$(M) = 1592 ($V_{\rm lim} \sim 21$) in an area of $65' \times 40'$ |
| Giants | $N$(RG) = 39 |
| (in an area of $65' \times 40'$) | $N$(RG-SB) = 12 |
| Blue Stragglers | $N$(BS) = 11 |
| $\delta$ Scuti | $N(\delta{\rm S}) = 7$ |
| Central stellar density | $\sigma = 0.72$ stars pc$^{-3}$ |
| | $\rho = 0.83$ M$_\odot$ pc$^{-3}$ |
| Cluster Mass | $M_{\rm tot} > 1400$ M$_\odot$ |